Supporting Information

Hou et al. 10.1073/pnas.1004143107

SI Materials and Methods

Animals, Tissues, and Retinal Thickness Measurement. PDGF-CC–deficient mice were bred onto C57Bl6 background for more than six generations and littermates were used for experiments. Even though the PDGF-C–deficient mice were postnatal lethal on a 129 background (1), they appear normal on a C57Bl6 background with no obvious phenotype. For eye tissue (choroid and retina) isolation, the anterior segment and the vitreous of the eyes were removed. The retina was dissected from the RPE-choroid-sclera (i.e., eye cup). The dissected tissues were put on dry ice immediately for RNA or protein analysis, or fixed for morphological analysis. For retinal thickness measurement, mice were euthanized. Eyes were marked at 12:00 at the corneal limbus and embedded in OCT compound and cryosectioned in parallel to the 12:00 meridian through the optic nerve. The sections were stained using the H&E method. Retinal thickness was measured at six locations: 25% (S1), 50% (S2), and 75% (S3) of the distance between the end of the peripheral retina and the optic nerve, and 25% (I1), 50% (I2), and 75% (I3) of the distance between the other end of the retina and the optic nerve.

Laser-Induced CNV Model and Fluorescein Angiography. Female mice (age 8–10 wk) were used for experiments. Four laser spots were made (75 μm spot size, 75 ms, 90 mW power; OcuLight Infrared Laser System 810 nm, Iridex) in the area surrounding the optic disk in the eye. Intravitreal injections of mouse PDGF-CC or VEGF shRNA (1 μg per eye; Open Biosystems), PDGF-CC or VEGF neutralizing antibody (2 μg per eye; R&D Systems and Angio-Proteomie, respectively) were performed immediately after laser treatment. For shRNA delivery, the transfection reagent in vivo-jetPEI (Polyplus Transfection) was used according to the manufacturer's instructions. For LiCl (Sigma) treatment, 1 μL per eye of 1 M stock solution was injected intravitreally immediately after laser treatment together with PDGF-CC–neutralizing antibody. The same amount and volume of NaCl was used as a control. CNV area was analyzed at 1, 2, or 3 wk after laser treatment using IB4 or H&E staining. Fluorescein angiography for blood vessel leakage analysis was performed as described (2). Briefly, 1 wk after laser-induced CNV, mice were anesthetized. FITC-dextran (100 μL; MW 40 kDa, 20 mg/mL; Sigma) in PBS solution was injected i.v. via tail vein during a period of 10 s. After 20 min, the eyes were enucleated and angiograms were obtained with a fluorescence microscope. Angiograms were graded as described (3): score of 0, no dextran leakage; 1, slight leakage; 2, moderate leakage; 3, intensive leakage. A typical photograph of each leakage score is shown in Fig. S7. Two examiners graded the leakage of the CNV lesions in a masked fashion and the average score was presented. When the two scores given for a particular lesion differ greatly, the sample was regraded and discussed until a similar result was reached.

ROP Model. The ROP model was described previously (4, 5). For antiangiogenic treatment in the retinal neovascularization assay, immediately after 5 d in hyperoxia, the mice received intravitreal injection of PDGF-CC–neutralizing antibody (2 μg per eye) or PDGF-CC shRNA (1 μg per eye). For shRNA delivery, the transfection reagent in vivo-jetPEI (Polyplus Transfection) was used according to the manufacturer's instructions. After 5 d in normoxia, the retinas were harvested for IB4 staining (Invitrogen) or gene expression analysis. Image analysis was performed by using a Z1 Imager and AxioVision software (Zeiss) as described previously (4).

Cell Culture, Cell Proliferation/Survival, Migration, and Real-Time PCR Assays. Primary adult hRPEs were isolated from two donor eyes as described previously (6). Cells were cultured in minimum essential medium with 10% FBS, nonessential amino acids, penicillin (100 U/mL), and streptomycin (100 μg/mL). Only cells between passages eight and 15 were used in the study. For monocyte purification, culture, and differentiation, peripheral blood monocytes were isolated from leukopheresed buffy coat fractions after density gradient centrifugation using Ficoll-Paque (Amersham Biosciences) according to the manufacturer's protocol. Anti-human CD14 (monocyte marker) microbeads (Miltenyi Biotec) were used for positive selection/purification of monocytes using an AutoMACS device (Miltenyi Biotec). CD14-positive cell purity was greater than 90%. Complete media (Biosource) consisting of RPMI 1640 supplemented with penicillin (100 U/mL), streptomycin (100 U/mL), L-glutamine (2 mM), and 10% FBS (HyClone) was used for monocyte culture. Macrophage colony-stimulating factor (Peprotech) was used to differentiate the monocytes into macrophages for 6 d. The cells were starved in complete medium with 0.2% FBS overnigh and then stimulated with 50 ng/mL PDGF-CC or BSA for 6 h, after which the cells were harvested for real-time PCR and Western blot analysis. Immortalized TR-rPCTs and TR-iBRBs were cultured as described previously (4, 7). Primary mCFs were isolated and cultured as described (8). HUVSMCs were purchased from American Type Culture Collection and cultured according to the manufacturer's instructions. For cell proliferation/survival assay, the cells were starved in serum-free medium overnight before the MTT assay (Invitrogen) was performed as previously described (4, 7). For the migration assay, confluent monolayer growth-arrested cells were wounded using a rubber policeman. The dishes were washed with serum-free medium and incubated for 16 h in serum-free medium containing the active form of human PDGF-CC–recombinant proteins or BSA (50 ng/mL). Each well was photographed at a magnification of 20×. Migration percentage corresponds to the ratio of the area of the cells migrated versus the total wound area. Real-time PCR assay and the primers used were described previously (4, 7).

CAM Assay and Immunofluorescence Staining. Fertilized eggs (CBT Farms) were incubated at 37.5 °C in a humidified incubator fitted with tilting shelves. At day 12, a window was made on the eggshell. PDGF-CC–neutralizing antibody (0.5 μg per egg; R&D Systems) or IgG air-dried on sterile glass coverslips were placed onto the CAM. The window was sealed with a parafilm and the eggs returned to the incubator. After 2 d, the microvasculature in and around the area covered by the glass slip was photographed using an Olympus microscope, and blood vessel branch points analyzed. Immunofluorescence staining for different samples was performed as described previously (4, 7). The antibodies used were: anti-PDGF-CC (9), rabbit antimouse collagen IV polyclonal antibody (2150-1470; AbD Serotec), rat antimouse Mac3 (BD Pharmingen), anti-SMA (M0851; Dako), and anti–phosphorylated PDGFR-α (sc-12911; Santa Cruz Biotechnology).

PDGFR-α, Akt, and GSK3β Expression/Phosphorylation Assay and Western Blot. PDGFR-α activation assay was performed as described previously (9). Briefly, cultured cells were stimulated with the active form of recombinant human PDGF-CC protein (9) at 50 ng/mL for 10 min and cell lysate subjected to further analysis. For IP assay, cell lysates were incubated with an anti–PDGFR-α antibody (sc-431; Santa Cruz Biotechnology) over-

night at 4 °C and precipitated with immobilized protein-G (Thermo Scientific). Immunoprecipitated samples were separated on a 10% SDS/PAGE and transferred to a PVDF membrane and were incubated with an anti-phosphotyrosine antibody (pY99; Santa Cruz Biotechnology). To detect activated and total Akt, antibodies against phosphorylated Akt (no. 9271; Cell Signaling Technology) and total Akt (no. 4685; Cell Signaling Technology) were used in Western blot assays. Other antibodies used for Western blot assays were: antimouse PDGF-CC (AF1447; R&D Systems), rabbit polyclonal PDGF-BB antibody (sc-7878; Santa Cruz Biotechnology), monoclonal anti–β-actin conjugated with HRP (A-3854; Sigma), anti-GSK3α/β (AF2157; R&D Systems), and anti–phospho-GSK3α/β (AF1590; R&D Systems).

Aortic Ring Assay. The aortic ring assay was performed as described (10). Briefly, aortas were excised from WT mice. The connective tissues surrounding the aorta were removed under a surgical microscope. Aortic rings (1 mm in length) were cut and rinsed five times with endothelial basal media (Lonza). Forty-eight–well plates were coated with 150 μL per well of basement membrane extract (BME; growth factor reduced; Cultrex). After gelling at 37 °C, an aortic ring was placed on top of the BME gel with 150 μL of BME added onto it. After 30 min, 500 μL of endothelial basal media containing PDGF-CC (9) (50 ng/mL) with or without DIF-3 (30 μM; Sigma-Aldrich) was added to each well. On day 12, images were taken using a phase contrast microscope equipped with a digital camera (Axiovert-20; Carl Zeiss). Images were converted to binary ones by application of a morphologic low-pass filter and threshold transformation using Adobe Photoshop CS3. The number of microvessels per field was counted in four fields surrounding the aortic ring where the highest microvessel density was found. The mean value of microvessel density of the four fields was used for each aortic ring.

Statistics. A two-tailed Student *t* test was used for statistical analysis. Difference was considered statistically significant when $P < 0.05$. The data are presented as mean ± SEM of the number of the determinations. Assays using cultured cells were performed in triplicate.

1. Ding H, et al. (2004) A specific requirement for PDGF-C in palate formation and PDGFR-alpha signaling. *Nat Genet* 36:1111–1116.
2. Tolentino MJ, et al. (2000) Angiography of fluoresceinated anti-vascular endothelial growth factor antibody and dextrans in experimental choroidal neovascularization. *Arch Ophthalmol* 118:78–84.
3. Takehana Y, et al. (1999) Suppression of laser-induced choroidal neovascularization by oral tranilast in the rat. *Invest Ophthalmol Vis Sci* 40:459–466.
4. Zhang F, et al. (2009) VEGF-B is dispensable for blood vessel growth but critical for their survival, and VEGF-B targeting inhibits pathological angiogenesis. *Proc Natl Acad Sci USA* 106:6152–6157.
5. Ritter MR, et al. (2006) Myeloid progenitors differentiate into microglia and promote vascular repair in a model of ischemic retinopathy. *J Clin Invest* 116:3266–3276.
6. Nagineni CN, Detrick B, Hooks JJ (1994) Synergistic effects of gamma interferon on inflammatory mediators that induce interleukin-6 gene expression and secretion by human retinal pigment epithelial cells. *Clin Diagn Lab Immunol* 1:569–577.
7. Li Y, et al. (2008) VEGF-B inhibits apoptosis via VEGFR-1-mediated suppression of the expression of BH3-only protein genes in mice and rats. *J Clin Invest* 118:913–923.
8. Klyve P, Nicolaissen B, Naess O (1996) Isolation and in vitro propagation of human choroidal fibroblasts. Morphology and characterization of the cultures. *Acta Ophthalmol Scand* 74:26–30.
9. Li X, et al. (2000) PDGF-C is a new protease-activated ligand for the PDGF alpha-receptor. *Nat Cell Biol* 2:302–309.
10. Kojima T, Chang JH, Azar DT (2007) Proangiogenic role of ephrinB1/EphB1 in basic fibroblast growth factor-induced corneal angiogenesis. *Am J Pathol* 170:764–773.

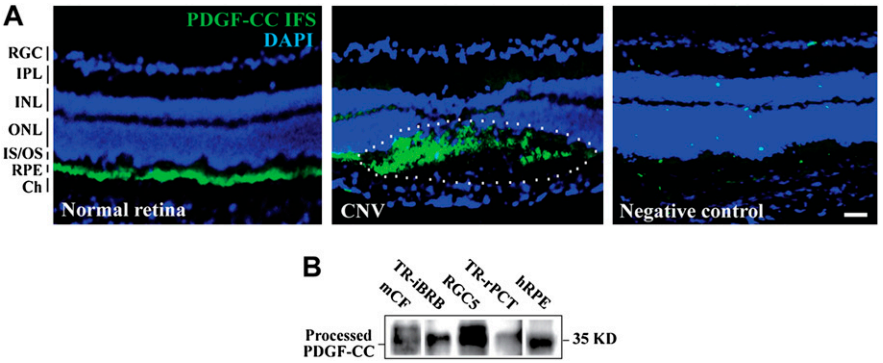

Fig. S1. PDGF-CC expression in CNV and cultured cells. (*A*) Immunofluorescence staining showed abundant PDGF-CC expression (green) within the CNV area (*Center*, lined area), whereas PDGF-CC was detected mainly in the RPE cells in normal retina (*Left*). (*B*) Western blot detected PDGF-CC expression in different types of choroidal and retinal cells, i.e., mCFs, TR-iBRBs, rat RGC-derived cell line (RGC5), TR-rPCT, and hRPEs. Blue color indicates nuclei stained by DAPI; IPL, inner plexiform layer; INL/ONL, inner/outer nuclear layer; IS/OS, inner/outer segments, Ch, choroid. (Scale bar: 25 μm.)

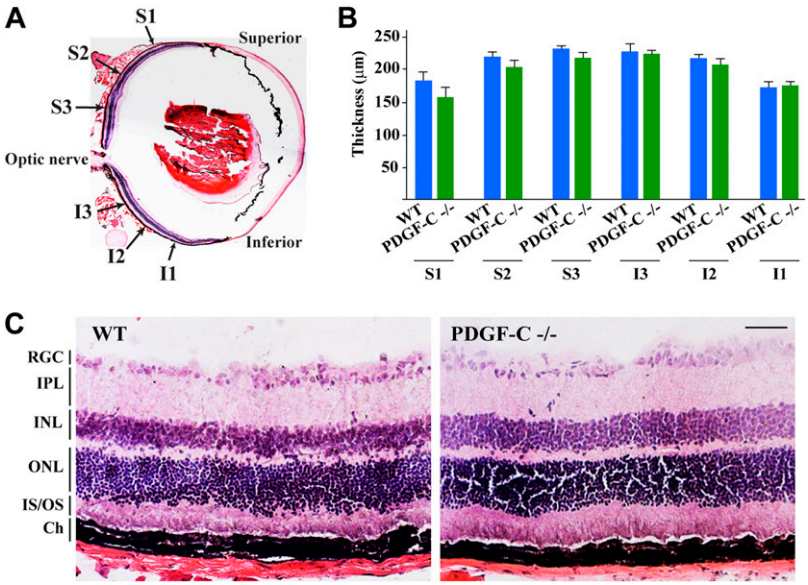

Fig. S2. Histological analysis using H&E staining did not show morphological difference between PDGF-CC–deficient and WT retinas and choroids. (*A*) Retinal thickness was measured in the PDGF-CC–deficient and WT retinas at six locations: S1, S2, and S3 in the superior retina and I1, I2, and I3 in the inferior part. (*B*) No significant difference in retinal thickness was found between PDGF-CC–deficient and WT retinas. (*C*) H&E staining did not show obvious morphological difference between PDGF-CC–deficient and WT retinas and choroids. IPL, inner plexiform layer; INL/ONL, inner/outer nuclear layer; IS/OS, inner/outer segments, Ch, choroid (Scale bar: 50 μm in *C*.)

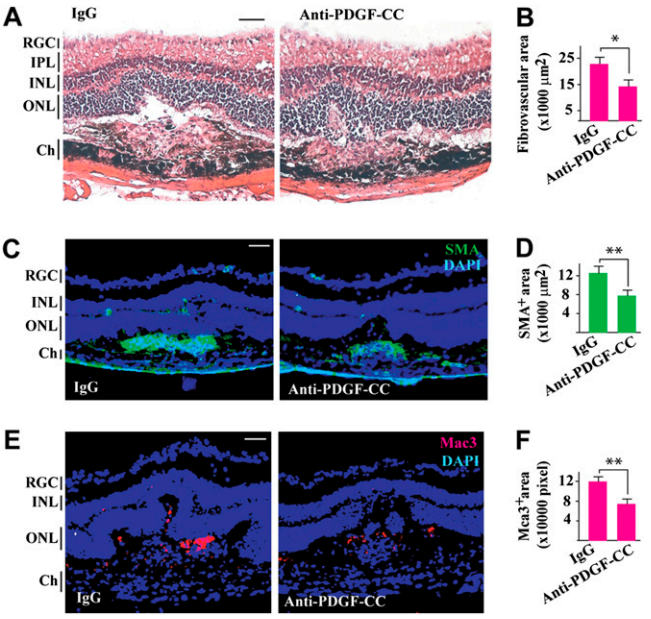

Fig. S3. PDGF-CC–neutralizing antibody inhibited CNV. (*A* and *B*) Treatment with PDGF-CC–neutralizing antibody decreased fibrovascular tissue formation in CNVs. (*C* and *D*) Treatment with PDGF-CC–neutralizing antibody decreased α-SMA (vascular smooth muscle cell marker)–positive areas (SMA^+) in CNVs. (*E* and *F*) Treatment with PDGF-CC–neutralizing antibody decreased Mac3-positive areas in CNVs. IPL, inner plexiform layer; INL/ONL, inner/outer nuclear layer; Ch, choroid. Blue color in *C* and *E* indicates nuclei stained with DAPI. (Scale bars: 50 μm.) $*P < 0.05$, $**P < 0.01$.

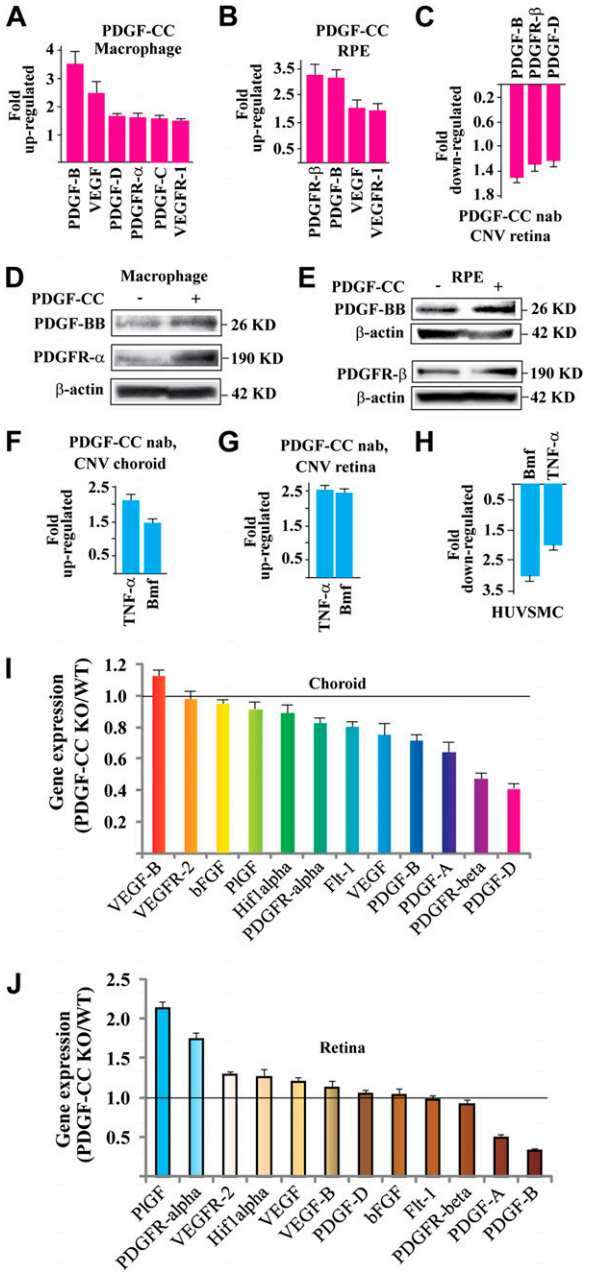

Fig. S4. PDGF-CC regulated expression of proangiogenic and proapoptotic genes. (*A* and *B*) PDGF-CC protein treatment up-regulated the expression of several important proangiogenic genes in cultured human primary macrophages and RPE cells as measured by real-time PCR. (*C*) Intravitreal injection of PDGF-CC–neutralizing antibody inhibited the expression of several important proangiogenic genes in the retinas with CNV in vivo as measured by real-time PCR. (*D* and *E*) Western blot confirmed that PDGF-CC protein treatment up-regulated the expression of several important proangiogenic genes in cultured primary human macrophages and RPE cells. (*F* and *G*) Intravitreal injection of PDGF-CC–neutralizing antibody up-regulated the expression of TNF-α and Bmf in choroids and retinas with CNV in vivo. (*H*) PDGF-CC protein treatment inhibited the expression of Bmf and TNF-α in cultured HUVSMCs. (*I*) PDGF-CC deficiency down-regulated the expression of PDGF-D, PDGFR-β, PDGF-A, and PDGF-B in normal adult mouse choroids. (*J*) PDGF-CC deficiency down-regulated the expression of PDGF-A and PDGF-B in normal adult mouse retinas.

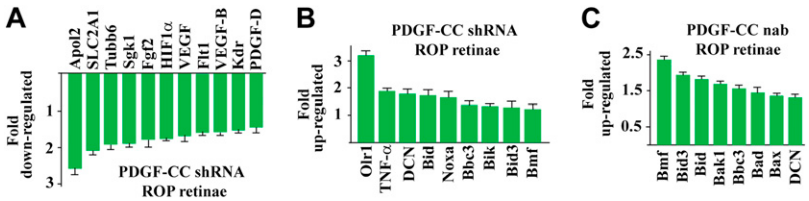

Fig. S5. PDGF-CC inhibition regulated the expression of proangiogenic and proapoptotic genes in the neovascular retinae. (*A* and *B*) Real-time PCR showed that PDGF-CC shRNA treatment decreased the expression of many proangiogenic genes (*A*) and increased the expression of many proapoptotic genes (*B*) in the neovascular retina in an ROP model. (*C*) PDGF-CC–neutralizing antibody treatment increased the expression of many proapoptotic genes in the neovascular retinas in an ROP mouse model.

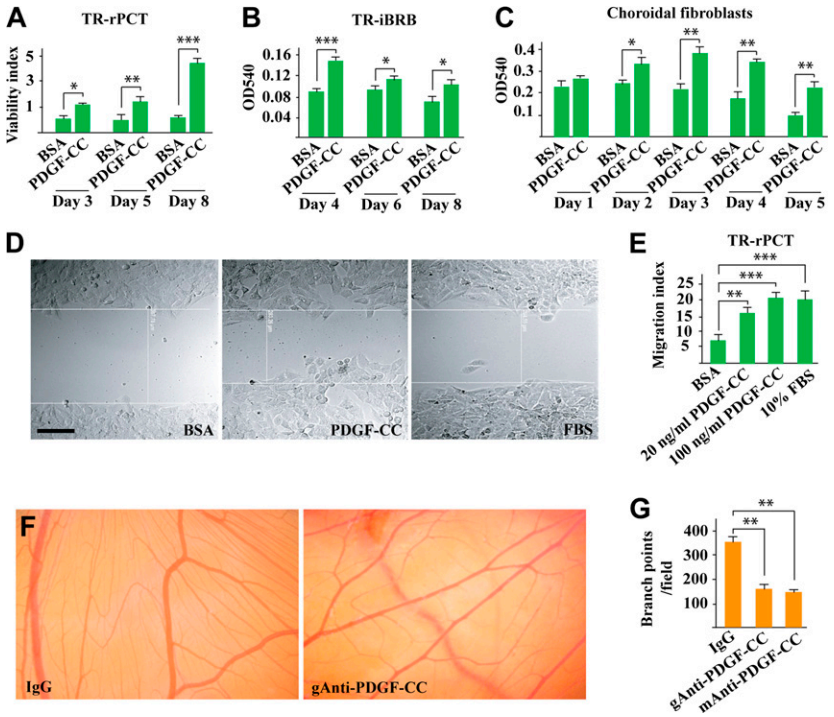

Fig. S6. PDGF-CC promoted vascular cell and fibroblast proliferation, survival and migration. (*A*–*C*) PDGF-CC protein increased proliferation/survival of TR-rPCT and TR-iBRB and mCFs at different time points. (*D* and *E*) In a monolayer cell migration assay, PDGF-CC protein promoted migration of the TR-rPCT cells at different concentrations. (Scale bar: 50 μm.) (*F* and *G*) In a chick CAM assay, PDGF-CC neutralizing antibody (gAnti-PDGF-CC) reduced blood vessel branch points 2 d after administration. $*P < 0.05$, $**P < 0.01$, $***P < 0.001$.

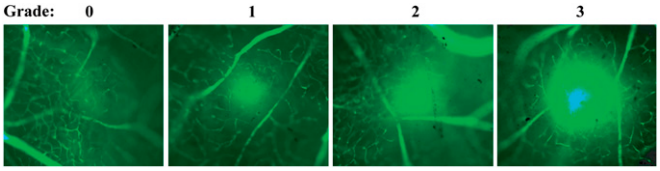

Fig. S7. Fluorescein angiography for blood vessel leakage analysis and grading. One week after laser-induced CNV, FITC-dextran (MW 40 kDa) in PBS solution was injected i.v. via tail vein. After 20 min, the eyes were enucleated and angiograms obtained by using a fluorescence microscope. Angiograms were graded as follows: score 0, no dextran leakage; 1, slight leakage; 2, moderate leakage; 3, intensive leakage.

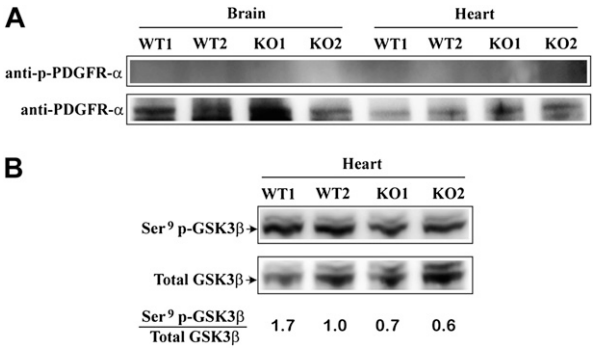

Fig. S8. PDGFR-α and GSK3β expression and activation in PDGF-CC–deficient tissues. (*A*) Western blot detected PDGFR-α protein in the PDGF-CC–deficient (KO) and WT brain and heart. An antibody against p-PDGFR-α (Tyr-754) did not detect PDGFR-α activation at Tyr-754 in WT or KO tissues; 75 μg of total protein was loaded in each lane. (*B*) Western blot detected GSK3β protein in the PDGF-CC–deficient (KO) and WT hearts. PDGF-CC–deficient hearts showed decreased GSK3β Ser^9 phosphorylation; 75 μg of total protein was loaded in each lane.